Parametric analysis with micro jitter generation for a direct current charging roller based electrophotographic device

Jeong Hoon Byeon[1] and Jang-Woo Kim[2,a)]
[1]*Department of Chemistry, Purdue University, West Lafayette, Indiana 47907, USA*
[2]*Department of Digital Display Engineering, Hoseo University, Asan 336-795, South Korea*

(Received 16 May 2011; accepted 21 June 2011; published online 29 July 2011)

To realize high quality electrophotography, it is important to clarify the influence of the design parameters in a charging roller (CR) system on the output image on the paper. We first analyzed the parameters related to the direct current (dc) bias CR system, and consequently confirmed micro jitter generation as a printing quality indicator for varying CR resistance and the surface roughness of the CR elastic layer. It turned out that the micro jitters were correspondingly generated for the chosen representative parameters, and therefore, the analyses can be used as a design platform to prepare an optimum dc CR system. © *2011 American Institute of Physics*. [doi:10.1063/1.3614495]

I. INTRODUCTION

The information technology industry is rapidly progressing and subsequently, with the advent of imaging technology,[1–4] electrophotographic systems became popular as digital printing devices because the systems have been the technology of choice for high speed printing.[5,6] Specifically, the systems have been applied and studied widely for office appliances to obtain a visible image fused on papers or transparencies.[4,7] In order to realize high-resolution electrophotographic systems such as laser beam printers, copying machines, and fax machines, it is important to clarify the influence of design parameters for a charging process consisting of gas discharge tools on the quality of the output image on the paper.[8–10]

The phenomenon of electrophotography is extensively used in applications based on static electricity, and is therefore particularly important.[11] A charging roller (CR) system is a kind of contact electrostatic charger for electrophotographic imaging devices. The system consists of a CR, an organic photoconductor (OPC), and a direct current (dc) power supply. The electrostatic charging happens between the CR and OPC, and thus the surface of the OPC is charged. The CR is made from graphite containing an elastic layer on a conductive shaft. The primary image-capturing element in an electrophotographic system, the OPC, is a thin layer of a dark-insulating, photoconductive material on a conductive cylinder.[12,13] Recently, this system has become popular because of greatly reduced ozone emissions compared with corona chargers.[14,15] Ozone is rarely generated by a dc bias CR system and this prevents the OPC, which is very sensitive to ozone, from degrading. The electrical discharge in an air gap formed close to the CR contact (or nip) area is the dominant component in the mechanism of electric charge movement from the CR to the OPC.[16] It is difficult to obtain uniform charging by a CR with a dc bias voltage and periodic charging patterns often can be observed on the OPC, especially by a single-layer CR with low resistance.[10] Because the periodic charging patterns degrade the quality of the printing image, they must be minimized and stable charging is desired. Thus, it is important to maintain the stability of the discharge for preventing image defects such as micro jitter (unwanted fine wrinkle patterns on the printed image, normally originating from charging instability) for high quality electrophotography. However, parametric analyses and experimental evidence for dc bias CR systems are still insufficiently reported. This is of interest in connection with the improvement of the charging performance in a laser beam printer. In this paper, design parameters were chosen for the CR system, which were numerically represented as charging maintenance and electric field distribution. Consequently, a selection of the analyzed results was compared with the experimental evidence (i.e., micro jitter on halftone printing image) to clarify their applicability in the design of a dc CR system.

II. EXPERIMENTAL DETAILS

Figures 1(a) and 1(b) show a schematic of the CR system with a DC bias voltage and the corresponding actual picture, respectively. The schematic consists of the CR, OPC (Mitsubishi Chemical Corporation), and dc power supply. The electrical discharge happens between the CR and OPC, and thus the surface of the OPC is electrostatically charged. From the dc CR schematic (Fig. 1(a)), the OPC surface potential (V_{OPC}) can be derived based on a Zener diode as follows:[17]

$$V_{OPC}(t) = \frac{Q_{OPC}}{C_{OPC}} = e^{-t/\tau}\frac{1}{\tau}\int_{t_0}^{t} e^{t/\tau}(V_a - V_P)\,\mathrm{d}t \qquad (1)$$

$$V_{OPC} = V_a - V_0 - S_P \cdot d_{\min} - V_\tau \ln\frac{V_a - V_0 - S_P \cdot d_{\min} + V_\tau}{V_\tau} \qquad (2)$$

where Q_{OPC} is the charge amount on the OPC local surface, C_{OPC} is the capacitance of OPC, t_0 and t are the initial and

a)Author to whom correspondence should be addressed. Electronic mail: jwkim@hoseo.edu.

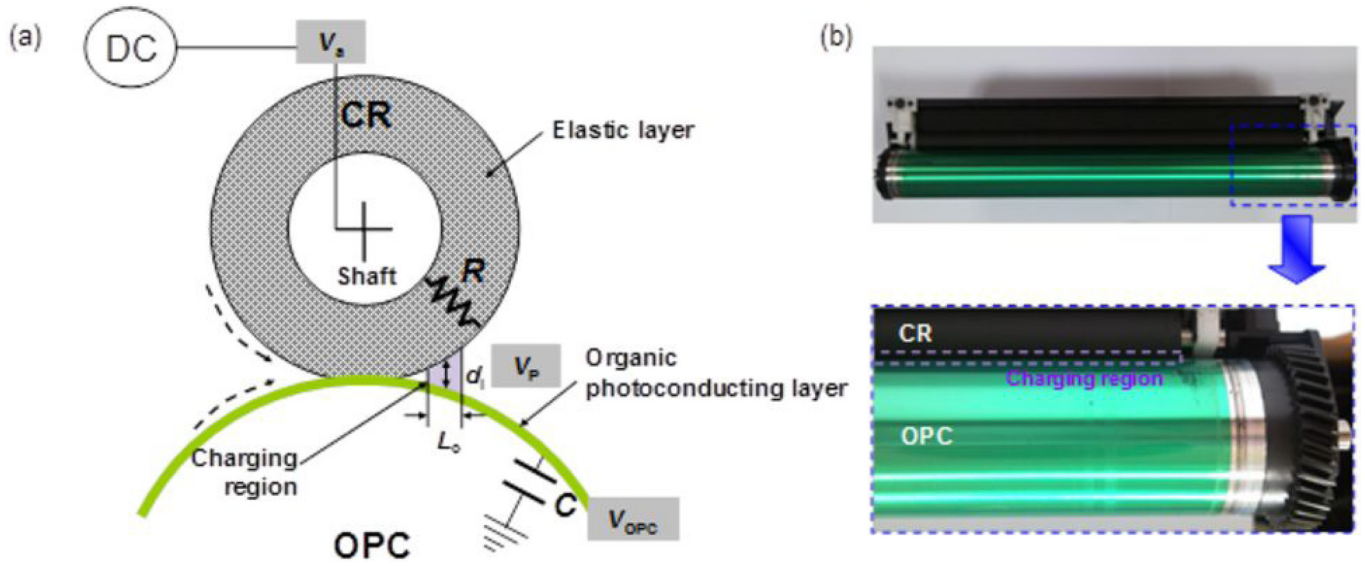

FIG. 1. (Color online) (a) CR system for parametric analyses. (b) Image of a CR system.

specific charging times respectively, and τ is the time constant (sec, C_{OPC} (F) $\times R_{CR}$ (Ω); where R_{CR} is the resistance of CR).[18] V_a is the applied voltage to the CR core shaft, V_P is the Paschen breakdown voltage in air, and V_0, S_P, and $d_{\min}$ are the minimum voltage ($\sim$230 V), curve slope ($\sim 10^4$ V mm^{-1}), and minimum gap distance ($\sim$7.5 μm) for the Paschen breakdown in air, respectively. V_τ is the systematic voltage, defined as follows:

$$V_\tau = S_P \cdot U_p \cdot \tau \cdot W_{nip} \cdot \frac{1 + r_{OPC}/r_{CR}}{2r_{OPC}} \tag{3}$$

where U_p is the process speed (mm sec^{-1}), W_{nip} is the width (mm) of the CR-OPC contact (or nip), and r_{CR} and r_{OPC} are the radii (mm) of the CR and OPC, respectively. The charging maintenance time (t_c) is derived by converting Eq. (1) as follows:

$$t_c = t_o - t_u = \tau \ln \frac{V_a - V_0 - S_P \cdot d_{\min} + V_\tau}{V_\tau} \tag{4}$$

where t_o is the overall time (sec) of a charging cycle, and t_u is the uncharging time in the cycle. The t_u term can be written as follows:

$$t_u = \frac{S_P \cdot d_{\min}}{V_\tau} \cdot \tau \tag{5}$$

Finally, the charging maintenance length (L_c) can be expressed as the product of the process speed and the charging maintenance time as follows:

$$L_c = U_p \cdot t_c \tag{6}$$

The end gap distance (d_o) of the charging roller can be expressed as follows:

$$d_o = \frac{V_\tau \cdot t_o}{S_P \cdot \tau} \tag{7}$$

The specifications of the experiments at normal temperature-normal humidity (denoted as 'NN': 22 °C, 55% relative humidity (RH)) environment are as follows: single-layer CR length of 230 mm; applied voltage of -1364 V; CR and OPC radii of 4.25 and 12 mm, respectively; nip width of 0.5 mm; process speed of 155 mm sec^{-1}; and OPC dielectric constant and thickness of 3 and 20 μm, respectively.

III. RESULTS AND DISCUSSION

Figures 2(a)–2(c) show the trends of the OPC surface potential (V_{OPC}), charging maintenance length (L_c), and specific charging gap distance (d_i) for varying parameters of the CR resistance (R_{CR}), CR-OPC nip width (W_{nip}), and CR radius (r_{CR}). Within the chosen range of the parameters, the change in V_{OPC}, L_c, and d_i for varying R_{CR} and W_{nip} is rather larger than those for varying r_{CR}. As the resistance was varied, L_c and d_i remarkably increased from about 0.6 MΩ of R_{CR} while V_{OPC} was inversely proportional to R_{CR}. Here, the L_c increase can be represented as a charging stability, and thus the experimental results (i.e., micro jitter generation on halftone printing image) correspondingly followed. For example, the results (Fig. 2(d)) clearly reveal that the R_{CR} has a large effect on the printing image quality; where micro jitter on the print image is enhanced by increasing the R_{CR} from 0.6 to 4.0 MΩ when -1364 V was applied to the CR core shaft.

The micro jitter generation is also verified with the surface roughness of the CR elastic layer; analytic (Figs. 3(a) and 3(b)) and experimental (Fig. 3(c)) results are depicted. In order to calculate the field (E) distribution between the CR and OPC surfaces, which is important for correlating between the surface roughness of the elastic layer and micro jitter generation, the field amplification factor (β) is used to account for the micro geometry of the surface of the elastic layer[19]:

$$E = \beta \cdot \frac{V_b}{d} \tag{8}$$

where β depends on the surface geometry, such as roughness. One way to calculate β is by using the simple approximation:

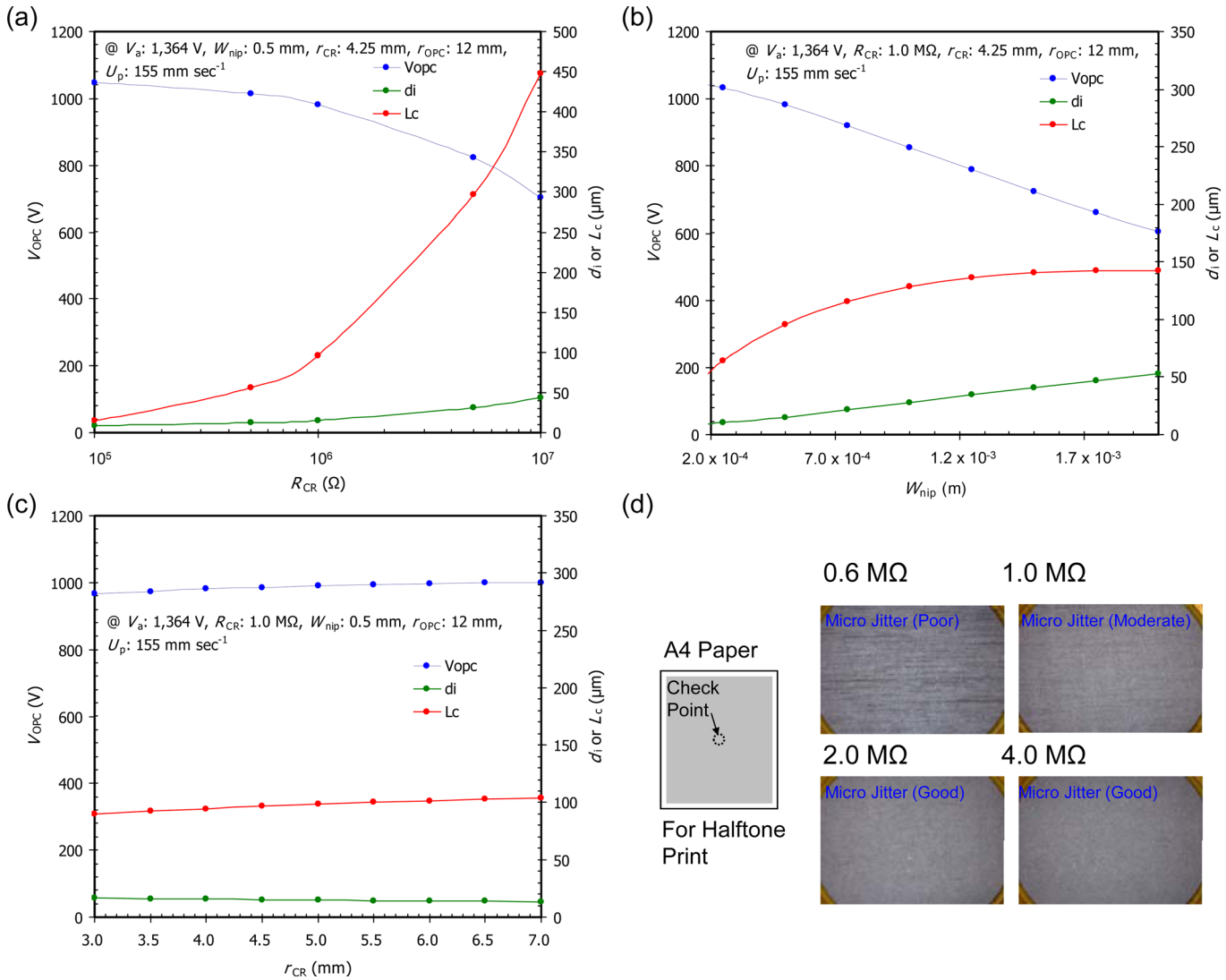

FIG. 2. (Color online) Results of parametric analyses (OPC surface potential (V_{OPC}), charging maintenance length (L_c), and gap distance (d_i)) and experiments (micro jitter on the printing image). (a) Function of CR resistance. (b) Function of nip width. (c) Function of CR radius. (d) Micro jitter generation vs CR resistance.

$$\beta \approx 2 + \frac{R_z}{R_a} \tag{9}$$

where R_z and R_a are the ten-point and arithmetic mean heights (μm) relating to the surface irregularity, respectively. V_b is the Paschen breakdown voltage, and is calculated as follows:

$$V_b = A \cdot \frac{p \cdot d}{B + \ln(p \cdot d)} \tag{10}$$

where p is the gas pressure (Pa), d is the gap distance (m), and A and B are the gas-dependent coefficients ($A = 279.6$ V m^{-1} Pa^{-1}, $B = 0.9$ for air). The uniformity of the field distribution is enhanced by decreasing the values of R_z (Fig. 3(a)) and R_a (Fig. 3(b)). Moreover, for varying R_a, the field magnification is also varied as well as the field distribution uniformity. Micro jitter generation is experimentally evaluated by the roughness variations, and the results including CR surface images are shown in Fig. 3(c). Regarding the analyses, the micro jitter generation is weak in accordance with decreasing R_z and R_a.

Additionally, we tested the micro jitter generation while varying the experimental environment for an identical CR-OPC specification (V_a of -1364 V, R_{CR} of 0.6 MΩ, W_{nip} of 0.5 mm, and r_{CR} of 4.25 mm), hence, the measured current (I)-voltage (V) characteristics including the approximation from Eq. (11) have been compared with the printing image quality,[10]

$$E_o \approx C \cdot \delta + D \cdot \sqrt{\delta / R_z} \tag{11}$$

where E_o is the discharge onset field (V m^{-1}), C (32.3×10^5 V m^{-1} in air) and D (0.846×10^5 V (m^{-1})$^{1/2}$ in air) are the uncertainty values, and δ is the relative air density. As shown in Fig. 4, the onset voltage (or onset field) for current generation decreased from the low temperature-low humidity (denoted as 'LL': 10 °C, 12% RH) to the high temperature-high humidity (denoted as 'HH': 32 °C, 85% RH) environment, and thus the linearity between V and I is rather

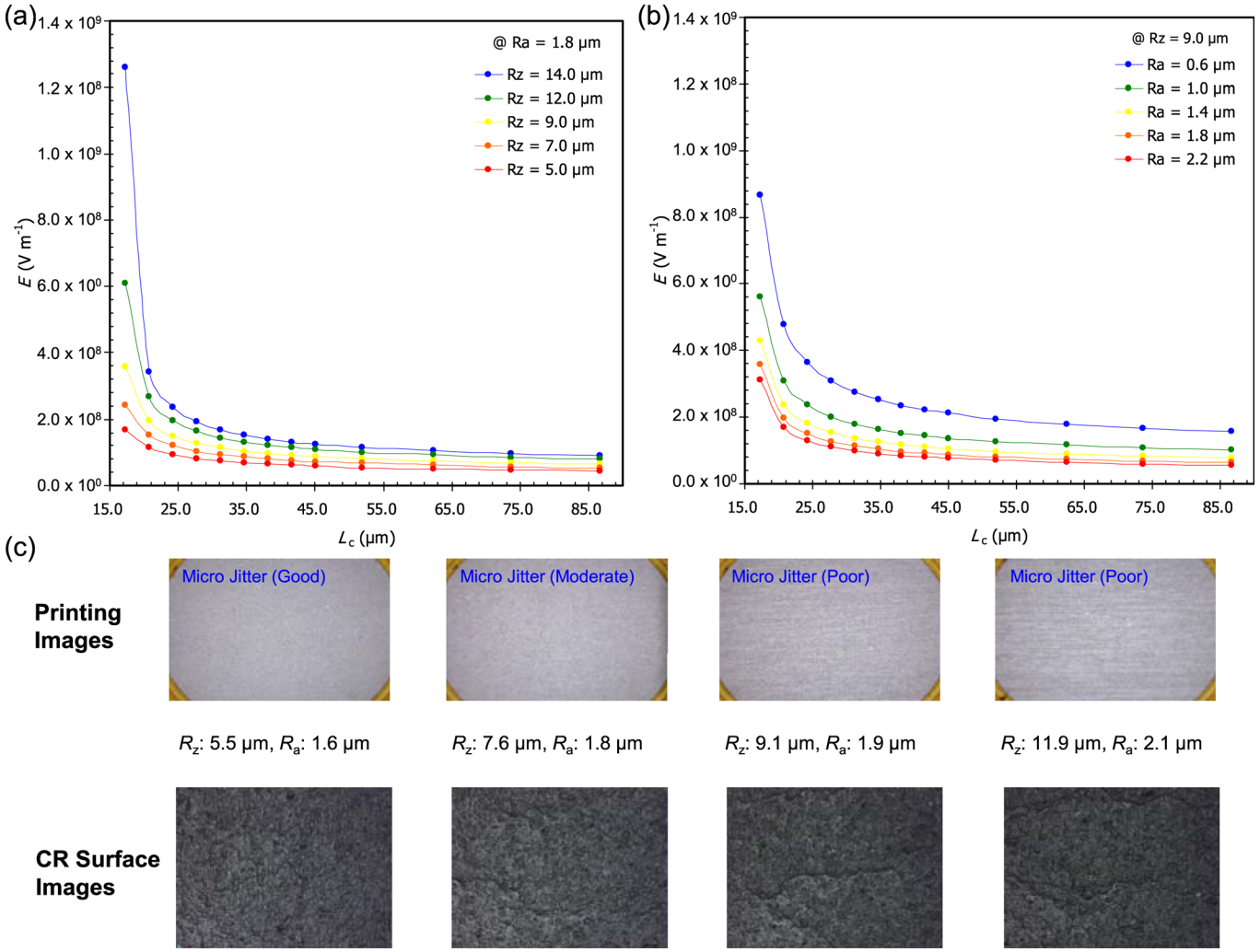

FIG. 3. (Color online) Parametric analyses for surface roughness of the CR elastic layer. (a) Field (E) distribution vs ten-point roughness (R_z). (b) E distribution vs arithmetic roughness (R_a). (c) Micro jitter generation vs R_z and R_a.

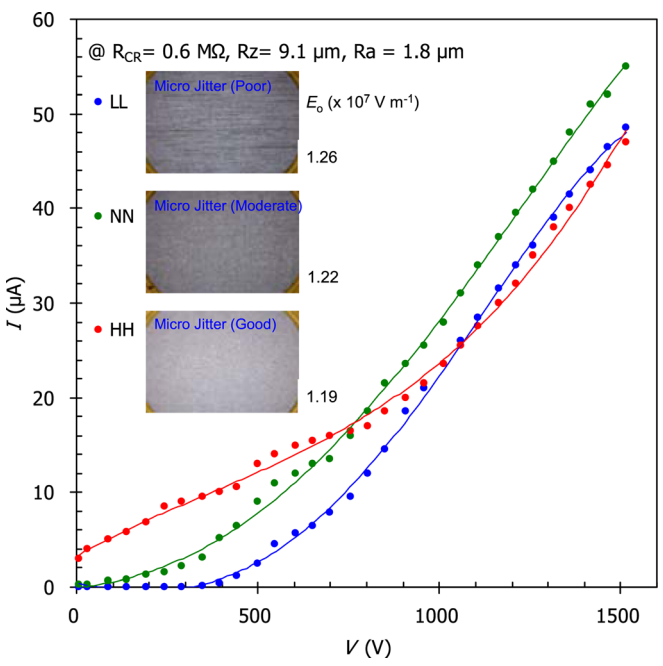

FIG. 4. (Color online) Sensitivity to micro jitter generation in the experimental environment.

enhanced for HH. More linear correlation can represent more stable charging (due to an enhanced charge flux onto the OPC), and thus the suppression of micro jitter generation is rather preferred for the HH environment than the others (see the insets of Fig. 4).

IV. CONCLUSIONS

In summary, the parameters related to the DC bias CR system (V_{OPC}, L_c, and d_i versus R_{CR}, W_{nip}, and r_{CR}) and the surface roughness of the CR elastic layer (E distribution versus R_z and R_a) were numerically analyzed, and subsequently confirmed micro jitter generation on the printing image for varying CR resistance and for surface roughness of the CR elastic layer. Results from the analysis and experiment clearly revealed that the R_{CR} has a large effect on the printing image quality; where micro jitter on the printing image is enhanced by increasing the R_{CR} from 0.6 to 4.0 MΩ. Regarding the surface roughness of the CR elastic layer, the micro jitter generation is weak in accordance with decreasing R_z and R_a (inducing uniformity of the E distribution). Additionally, micro jitter generation while varying the experimental environment for an identical CR-OPC specification is

verified, and the generation is affected by the environment in accordance with the *I-V* characteristics. Our strategy of parametric analyses along with gathering evidence through experiments is attractive because of its simple and distinctive features, and it may contribute to appropriately designing dc bias CR systems in electrophotographic devices.

[1]G. Bartscher, S. O. Cormier, R. Lyness, and L. B. Schein, J. Electrost. **53**, 295 (2001).
[2]D. S. Rimai, D. S. Weiss, M. C. de Jesus, and D. J. Quesnel, C. R. Chim. **9**, 3 (2006).
[3]L. B. Schein, J. Vac. Sci. Technol. A **25**, 1256 (2007).
[4]K.-S. Choi, T. Fujiki, and Y. Murata, Jpn. J. Appl. Phys. **43**, 7693 (2004).
[5]C.-L. Chen and G. T.-C. Chiu, Mechatronics **18**, 412 (2008).
[6]H. Mio, R. Higuchi, W. Ishimaru, A. Shimosaka, Y. Shirakawa, and J. Hidaka, Adv. Powder Technol. **20**, 406 (2009).
[7]C.-S. Lee, J.-Y. Park, E.-S. Cho, H.-J. Lee, M.-H. Kim, and J.-N. Yoo, J. Imaging Sci. Technol. **41**, 600 (1997).
[8]H. Fusayasu, H. Inoue, Y. Komatsu, and Y. Sekine, IEEE Trans. Magn. **37**, 3440 (2001).
[9]H. Kawamoto and S.-I. Serizawa, J. Imaging Sci. Technol. **41**, 629 (1997).
[10]J.-S. Chang, A. J. Kelly, and J. M. Crowley, *Handbook of Electrostatic Processes* (CRC Press, New York, 1995), p. 321.
[11]H. Okada, D. Shindo, J. J. Kim, Y. Murakami, and H. Kawase, J. Appl. Phys. **102**, 054908 (2007).
[12]R. H. Young, J. Appl. Phys. **72**, 2993 (1992).
[13]Y. Kanemitsu, H. Funada, and S. Imamura, J. Appl. Phys. **67**, 4152 (1990).
[14]M. Kadonaga, T. Katoh, and T. Takahashi, J. Imaging Sci. Technol. **43**, 274 (1999).
[15]H. Hirakawa and Y. Murata, Jpn. J. Appl. Phys. **33**, 4102 (1994).
[16]M. Yamamoto, Y. Takuma, K. Kikuchi, and T. Miyasaka, Imaging Science & Technology, NIP20 Int. Conf. Digital Printing Technol., Society for Imaging Science and Technology, Springfield, 2004), p. 12.
[17]S. Wong, C. Hu, and S.-P. Chan, Int. J. Electron. **71**, 309 (1991).
[18]D. Landheer, J. Appl. Phys. **51**, 1809 (1980).
[19]R. G. Longwitz, PhD dissertation, Faculty of Sciences and Techniques, EPFL, Lausanne, 2004.